

Discontinuous rigidity transition associated with shear jamming in granular simulations

Varghese Babu,^{1,*} H. A. Vinutha,² Dapeng Bi,³ and Srikanth Sastry^{1,†}

¹*Jawaharlal Nehru Center for Advanced Scientific Research, Jakkur Campus, Bengaluru 560064, India.*

²*Department of Physics, Institute for Soft Matter Synthesis and Metrology, Georgetown University, Washington, DC, USA.*

³*Department of Physics, Northeastern University, MA 02115, USA*

(Dated: January 31, 2023)

We investigate the rigidity transition associated with shear jamming in frictionless, as well as frictional, disk packings in the quasi-static regime and at low shear rates. For frictionless disks, the transition is under quasistatic shear is discontinuous, with an instantaneous emergence of a system spanning rigid cluster at the jamming transition. For frictional systems, the transition appears continuous for finite shear rates, but becomes sharper for lower shear rates. In the quasi-static limit, it is discontinuous as in the frictionless case. Thus, our results show that the rigidity transition associated with shear jamming is discontinuous, as demonstrated in a past for isotropic jamming of frictionless particles, and therefore a unifying feature of the jamming transition in general.

Granular materials can exist in a flowing or a solid state. The transition between these states, called the jamming transition, has been the subject of intense research [1–3], particularly under isotropic compression of frictionless sphere packings. The jamming point ϕ_J for packings of soft particles exhibits many characteristics of a second-order phase transition, at which various quantities show power law scaling – with respect to the distance from the jamming point – as one compresses beyond the jamming point [4, 5]. Further, the distribution of small forces between particles just in contact, as well as the gaps between particles nearly in contact, also exhibit power law behavior. Exponents characterizing these are constrained by an inequality that is saturated for configurations at the jamming point, which are therefore “marginally stable” [6, 7]. The mean-field theory of glasses and jamming has predictions for these exponents which match numerical values for dimensions $D = 2$ and above [5]. Extensions of this theory predict these exponents to be the same for shear jamming, as recent numerical results indeed confirm, along with the aforementioned aspects of criticality [8]. These and related results [8, 9] strongly support a unified description of both isotropic and shear jamming.

In contrast, the manner in which the contact network acquires rigidity is strongly discontinuous [10, 11] for frictionless isotropic jamming. At the jamming point, the entire system (barring a small percentage of *rattlers*, described later) acquires rigidity discontinuously. From the Maxwell criterion for the rigidity of networks of nodes connected by edges representing distance constraints, the contact network of a configuration with N particles in D dimensions can be rigid when contacts result in at least $N_c = D(N - 1)$ constraints on the non-global degrees of freedom. In general, this is a necessary but not sufficient condition. Therefore, isotropic jamming occurs at the *isostatic point*, where the system has just the minimum number of contacts per particle, Z required, $Z_{iso} = 2D$ (from $\frac{NZ_{iso}}{2} = ND$). This discontinuous rigidity transi-

tion is different from the continuous transition observed, *e. g.* for *sticky* packings [12, 13], and in random spring networks [14, 15] for which the rigid component of the system grows continuously beyond rigidity percolation, which does not occur at the isostatic point, and is preceded by the presence of both rigid and over-constrained regions.

Results available for shear jamming appear to suggest that the rigidity transition is continuous, in contrast to isotropic jamming [16–19]. Computational investigation of the rigidity transition for frictional two dimensional ($2D$) systems sheared at finite rates [16] revealed a broad distribution of rigid cluster sizes with increasing mean size as the jamming transition is approached, supporting a continuous rigidity transition, although becoming “sharper” as the shear rate is lowered. Similar results have been recently reported from analysis of sheared granular packings in experiments [18]. Following the observation that sheared *frictionless packings* acquire geometric characteristics associated with jamming [20], the rigidity transition in such packings in $2D$ was analysed by including constraints associated with friction [19]. The size distribution of overconstrained clusters, similar to [16], exhibits a broad distribution, supporting a continuous rigidity transition. In addition, the rigidity transition associated with jamming in frictional systems were studied in lattice models of jamming where a continuous transition was observed except in a limiting case corresponding to infinite friction [17].

These observations suggest that the nature of the rigidity transition could be an exception to the commonality of isotropic and shear jamming phenomenology outlined earlier. In this letter, we therefore investigate carefully the nature of the rigidity transition for both sheared frictional and frictionless packings, under both quasi-static and at finite shear rate. We find that the rigidity transition is unambiguously discontinuous under quasistatic shear. Such a transition appears rounded in the case of finite shear rate, but the dependence on shear rate clearly

supports an approach to a discontinuous transition in the limit of vanishing shear rate.

Shear jammed frictionless packings are obtained by shearing unjammed bidisperse soft-disk mixtures of size ratio 1 : 1.4 above the minimum jamming density ϕ_J . As described in [8, 21–23], well annealed disk-packings jam at a packing fraction higher than ϕ_J . In this study, we equilibrate hard-disk configurations at high density, which jam at a density $\phi_j > \phi_J$ with the protocol described in [4]. Unjammed configurations decompressed to a density ϕ , with $\phi_J < \phi < \phi_j$ undergo shear jamming when subjected to athermal quasistatic shear (AQS) wherein strain increments of $\Delta\gamma = 5 \times 10^{-4}$ are applied, each step followed by energy minimization. We study 3 independent samples of $N = 16384$ particles at a density of $\phi = 0.8485$, with $\phi_j \approx 0.85$ and $\phi_J \approx 0.84$.

We use Discrete Element Method (DEM) [24] to simulate frictional disks, using LAMMPS [25], with linear and tangential spring dash-pot forces. The model includes damping in both normal and tangential directions, in addition to global viscous damping. The normal and tangential spring constants k_n and k_t are set to 2.0. The normal velocity damping η_n is set to 3.0 and the tangential damping η_t is set to $\frac{1}{2}\eta_n$. The global damping term η is also set to ≈ 3 .

Shear is applied by performing an affine transformation of particle positions, with strain increments $\Delta\gamma$ followed by relaxation using DEM. Because of the damping terms, the system will eventually reach a force, torque balanced configuration if one waits long enough. Quasistatic shear requires reaching force/torque balance at each strain step. In practice, we consider the system to have reached force/torque balance when the total force (sum of total forces acting on the disks) is less than 10^{-11} or when the total kinetic energy of the system is less than 10^{-19} . The simulation is stopped when the number of timesteps reaches 2×10^9 regardless. The timescale required to relax the system diverges at the shear jamming transition as pointed out in [26] and thus it is difficult to achieve force-balance close to the transition. For a finite shear rate $\dot{\gamma}$, each strain step is followed by DEM dynamics of duration $\Delta\gamma/\dot{\gamma}$. We set $\Delta\gamma$ is 10^{-4} for finite rate shear and 10^{-3} for quasi-static shear. We perform finite rate shear on a system size of $N = 16384$ particles for 10 independent samples (and 20 samples for highest and lowest shear rate), and quasi-static shear with $N = 2000$ for 16 samples. The packing fraction ϕ of the system is 0.81. Further details of the simulations are described in the supplemental material (SM) section I [27]. We describe the results for friction coefficient $\mu = 1$ in the main text. Results with $\mu = 0.1$ can be found in SM section V.

A major distinction between frictionless and frictional jamming is the isostatic contact number Z at which jamming can occur in the absence of redundant constraints, which has been shown to range from $D + 1$ to $2D$ de-

pending on the friction co-efficient μ [19, 20, 28, 29] with $Z_{iso} = D + 1$ for $\mu = \infty$. This can be understood using the generalized isostaticity condition, obtained by considering additional conditions due to the ‘‘mobilized contacts’’[28]. The tangential frictional force between two particles has an upper bound due to the Coulomb threshold: $f_t \leq \mu f_n$ and the mobilized contacts are those for which $\frac{f_t}{f_n} \approx \mu$. Considering a configuration with N particles and $n_m N$ mobilized contacts, the conditions that the contact network at jamming has to satisfy are DN force balance conditions, $\frac{D(D-1)}{2}N$ torque balance conditions and $n_m N$ Coulomb conditions. The number of constraints imposed by the contacts is $\frac{NDZ}{2}$ (since each contact constrains one translational and $D - 1$ rotational degrees of freedom). Z is by default computed excluding *rattlers* (particles with less than the minimum number of contacts necessary for local rigidity, = 3 for frictionless, and 2 for frictional particles in 2D), and represented by Z_{NR} for clarity. Defining $Z_\mu = Z_{NR} - \frac{2n_m}{D}$, the generalized iso-staticity condition is

$$Z_\mu^{iso} = Z_{NR} - \frac{2n_m}{D} = D + 1. \quad (1)$$

For $2D$ networks arising in several contexts including jamming, the onset of rigidity has been analysed by employing the pebble game algorithm[14]. Each node of the network represents a disk in the present context and is assigned k pebbles ($k = 2$ for frictionless disks and $k = 3$ for frictional disks) representing the degrees of freedom. The constraints imposed by each contact are represented by 1 or 2 edges (2 for the frictional case, 1 for the frictionless case, as well as for a mobilised contact). A (k, l) pebble game ($l = 2$ indicates the global degrees of freedom) assigns pebbles recursively to edges, and based on such an assignment, decomposes the network into rigid clusters that are mutually floppy. Rigid clusters with redundant bonds (with no assigned pebbles) are termed over-constrained. A more detailed description of the algorithm is provided in SM section II. We employ the pebble game to monitor the size of the largest rigid cluster in the system primarily, as well as the distribution of the size of rigid clusters.

First, we discuss the results of the frictionless system, for which above jamming, energy minimization cannot remove all the overlaps in the system, resulting in finite forces. As discussed in [8, 21], configurations are isostatic ($N_c = (N - 1) \times 2$ after removing rattlers) at the jamming point. ($k = 2, l = 2$) pebble game analysis of isostatic configurations shows that the whole system is made up of a single rigid cluster, as shown in Fig. 1 (a). Removing a single bond from this system leads to loss of rigidity, as shown in Fig. 1 (b). The results of this analysis are summarized in Fig. 2. The shear jamming transition can be identified by the presence of finite contact forces as well as by Z_{NR} . The rigidity transition occurs at the jamming transition point and

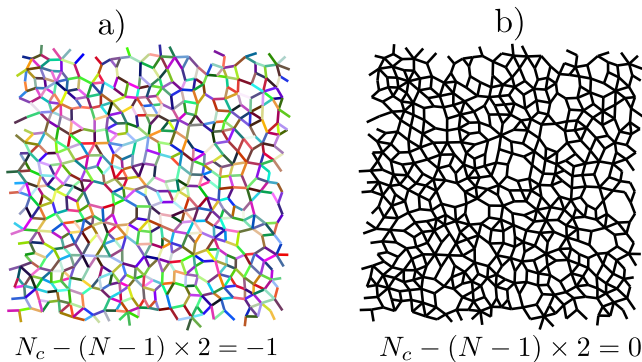


FIG. 1. **Rigidity transition in sheared frictionless disk packings.** Pebble game analysis on the isostatic networks yields a single rigid cluster consisting of the whole system (b). Removal of one bond from that network results in a complete loss of rigidity, with the pebble game decomposing the system into multiple small rigid clusters indicated by the different colors (a).

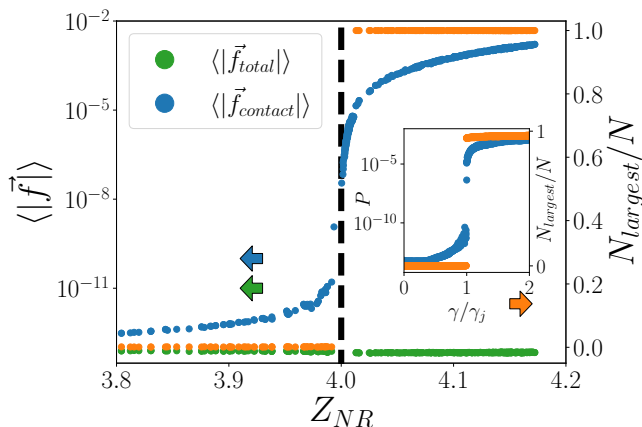


FIG. 2. **Rigidity transition associated with shear jamming in frictionless systems.** Rigidity transition can be seen as a discontinuous jump in the size of the largest cluster. Inset shows pressure P vs strain γ and the rigidity transition. The transition occurs at the isostatic value of the non-rattler contact number, $Z_{NR} = 4$.

is characterized by a discontinuous jump in the size of the largest cluster. This strongly discontinuous rigidity transition is therefore common for frictionless isotropic and shear jamming.

Next, we discuss the results from finite rate shear of frictional systems for shear rates $\dot{\gamma} = 10^{-6}, 10^{-7}, 10^{-8}, 10^{-9}, 10^{-10}$. The main observation from this set of simulations is that the rigidity transition associated with shear jamming becomes “sharper” as one reduces the shear rate, an observation also made in [16]. As shown in Fig. 3 (a), the increase in pressure P with strain is noticeably sharper for smaller shear rates. To characterize the rigidity of these configurations we follow [16, 18, 19] and use the ($k = 3, l = 2$) pebble

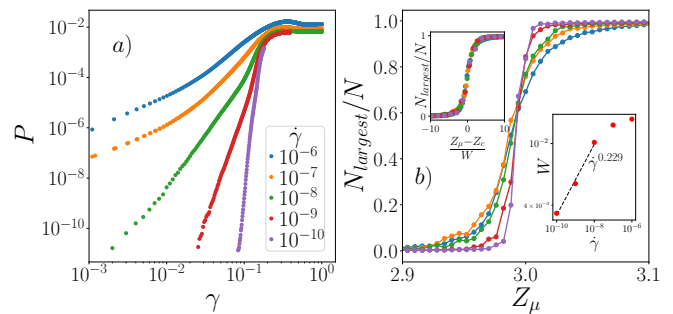


FIG. 3. **Finite rate shear for $N = 16384$ with $\mu = 1$.** a) Pressure P vs γ . b) Fraction of the largest rigid cluster with the total number of particles as a function of Z_μ . As $\dot{\gamma}$ is reduced the transition becomes “sharper”. **Inset top left:** Data from different shear rates collapse onto each other when scaled by the “width” W of the transition region. **Inset lower right:** The width of the transition region obtained by fitting the data. Dependence of W for the three smaller shear rates on $\dot{\gamma}$ can be described using a power-law suggesting that the transition becomes discontinuous as $\dot{\gamma} \rightarrow 0$.

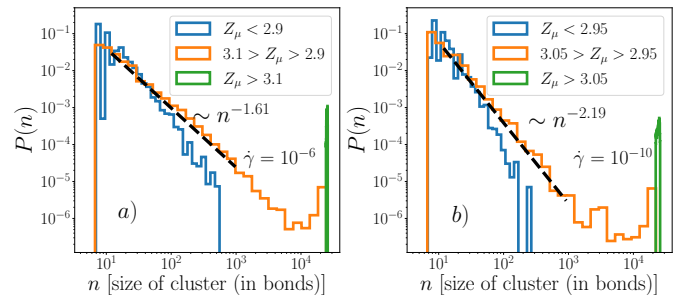


FIG. 4. **Comparison of cluster size distribution between high and low $\dot{\gamma}$ studied.** a) $\dot{\gamma} = 10^{-6}$ and b) $\dot{\gamma} = 10^{-10}$. Comparing the distribution of cluster sizes for the range covering 3, we see that $\dot{\gamma} = 10^{-6}$ shows a broader distribution compared to the one at $\dot{\gamma} = 10^{-10}$ as quantified by the exponent characterizing the power law distribution, indicating that the transition becomes discontinuous as the shear rate vanishes. The distribution corresponding to a given region in Z_μ is calculated by considering the sizes of all rigid clusters in a configuration with Z_μ in that region.

game on the contact network. Note that in the finite rate simulations, we do not simulate the system till it achieves force balance, and therefore for jammed as well as unjammed configurations, the net forces on the disks are finite. We use a threshold δ to identify mobilized contacts - if $\frac{|\vec{f}_i|}{|\vec{f}_n|} > \mu - \delta$ then the contact is mobilized. For simulations with $\mu = 1$, very few of our contacts are sliding and the choice of δ does not significantly affect the results presented. The choice $\delta = 10^{-12}$ for the results in the main text. A discussion on the choice of δ is included in the SM section VI. Even though the system is not in force balance when sheared at a finite rate, we identify rattlers as particles with just one contact and

remove them recursively. For the remaining contact network, we perform pebble game analysis and show in Fig. 3 (b) the size of the largest rigid cluster as a function of the average contact number $Z_\mu = Z_{NR} - n_m$. The transition becomes sharper as one reduces $\dot{\gamma}$, and interestingly, the transition occurs at $Z_\mu \approx 3$, the isostatic value, for all shear rates. We fit the data using the logistic function $f(x) = \left[1 + e^{-\frac{x-Z_c}{W}}\right]^{-1}$ (as a reasonable but arbitrary choice) and use W as a measure of the width of the transition region. As the top left inset in 3 (b) shows, the data can be collapsed using the fit values, with $Z_c \approx 2.99$. In the lower right inset, we show the behavior of W , whose dependence on $\dot{\gamma}$ can be described by a power law that implies that the transition becomes discontinuous at $\dot{\gamma} \rightarrow 0$. To our knowledge, this has not been reported for shear jamming transition.

Next, we study the cluster size distribution as shown in Fig. 4 for the largest and the smallest $\dot{\gamma}$ studied. For both cases, we divide the region studied (in Z_μ) into three regimes – before the jamming transition, a regime covering the transition, and after the transition – and compute the distribution of the rigid cluster sizes separately for each of them. The distributions in the regime covering the transition are quantified by an exponent characterizing the power-law distribution of the rigid clusters. For $\dot{\gamma} = 10^{-6}$, the exponent is -1.61 and for $\dot{\gamma} = 10^{-10}$, the exponent is 2.19 . While the transition in this regard appears continuous for both the shear rates studied, the distributions become progressively narrower as the shear rate decreases. The corresponding curves for the frictionless and frictional quasistatic shear show a faster than power law decay below the rigidity transition. We also calculate P_∞ , the probability that a given disk belongs to a system spanning (percolating) rigid cluster, which is shown in the SM section IV. The P_∞ curves become progressively step-like with decreasing shear rate. Thus, we conclude that the appearance of a continuous transition is associated with the finite shear rates and absence of force/torque balance, rather than being an indication of the intrinsic nature of the shear jamming transition, or the presence of friction.

To underscore our conclusions, we next consider quasistatic shearing of frictional disks, which is performed by applying an affine transformation and relaxing the system using DEM till the system reaches force balance. As noted before, the relaxation near the jamming transition is very slow and therefore it is hard to generate force-balanced configurations near the jamming transition [26, 30]. Given configurations that are fully relaxed, we define rattlers as particles that do not have finite forces acting on them. Disks with a single contact cannot sustain a non-zero force on that contact, which we remove recursively. In addition, given a friction co-efficient μ , disks with two contacts can be in force balance with finite forces only if the angle θ between the two contacts

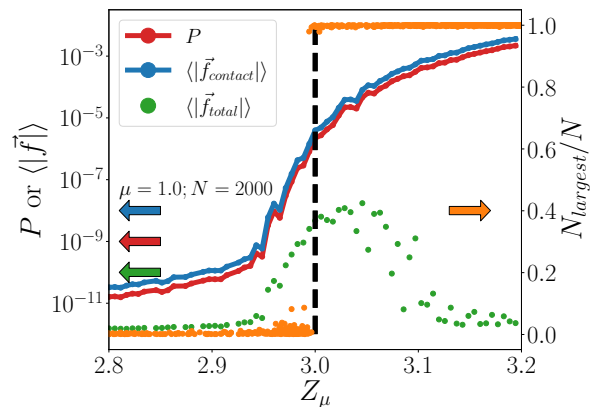


FIG. 5. **Rigidity analysis of quasi-statically shear jammed frictional disks.** The size of the largest rigid cluster discontinuously jumps to equal the system size as Z_μ crosses 3, the iso-static value. The contact forces and pressure show a more gradual change, but the behavior of the net force on the disks reveals this to be a result of incomplete convergence, as indicated by the average of the net force of individual disks.

is large enough. If $\mu < \tan(\frac{\pi}{2} - \frac{\theta}{2})$, these contacts cannot carry forces (see SM section III), and are this also removed recursively.

These configurations are analyzed using the ($k = 3, l = 2$) pebble game, and the results are shown in Fig. 5. As Z_μ crosses the isostatic value 3, the largest rigid cluster encompasses the whole system, exhibiting a striking similarity with the behavior found for the frictionless case (Fig. 2). This observation is even more remarkable when one considers the behavior of the contact forces or pressure, *vs.* Z_μ , which show a more rounded change, as a result of the difficulty of converging to force balanced configurations, as indicated by the non-monotonic behavior of the net forces acting on the disks. P , $\langle |\vec{f}_{contact}| \rangle$ and $\langle |\vec{f}_{total}| \rangle$ shown are average values computed from all configurations having a given value of Z_μ . $N_{largest}/N$ is a scatter plot from all trajectories.

Before closing, we briefly compare our results and conclusions with previous work mentioned earlier. While the conclusion in [16] differ from ours, the sharpening of the rigidity transition has also been noted in [16]. In [19], shear was applied to frictionless disk assemblies before friction was included in the rigidity analysis. While this procedure captures many features of sheared frictional disks, like the anisotropy and the emergence of a contact network that supports jamming in the presence of friction, subtle but important differences in the organization of contacts exist. Specifically, using the procedure of [19], the fraction of redundant bonds rises continuously from below the isostatic contact number, as shown in the SM Section VII, whereas they are strictly zero below the frictional jamming point. The absence of redundant bonds before the rigidity transition is a characteristic feature of

jamming, as compared to rigidity percolation in spring networks and other systems [15]. Our results differ from the analysis of experimentally sheared disk packings in [18], for which we do not have a ready explanation, since the experimental protocol should be expected to closely agree with the quasistatic shear we employ, an inconsistency that needs to be further investigated.

In summary, our results unambiguously demonstrate that the rigidity transition associated with shear jamming in both frictionless and frictional disk packings is discontinuous in nature, when conditions of force and torque balance are met. Thus, the nature of the emergence of rigidity is the same for isotropic and shear jamming. Features that suggest a continuous transition are associated with partial relaxation of unbalanced forces, as our results for finite shear rate demonstrate, but such behavior approaches discontinuous change as the shear rate vanishes. Our results thus establish a key additional element in the shared phenomenology of isotropic and shear jamming.

We thank Sumantra Sarkar, Sanat Kumar, Karen Daniels and Silke Henkes for useful discussions. We acknowledge support from the Thematic Unit of Excellence on Computational Materials Science (TUE-CMS) and the National Supercomputing Mission facility (Param Yukti) at the Jawaharlal Nehru Centre for Advanced Scientific Research (JNCASR) for computational resources. D.B. acknowledges support from the National Science Foundation (grant no. DMR-2046683) and the Alfred P. Sloan Foundation. S.S. acknowledges support through the JC Bose Fellowship (Grant No. JBR/2020/000015) from the Science and Engineering Research Board, Department of Science and Technology, India.

* varghese@jncasr.ac.in

† sastry@jncasr.ac.in

- [1] Robert P Behringer and Bulbul Chakraborty. The physics of jamming for granular materials: a review. *Reports on Progress in Physics*, 82(1):012601, 2018.
- [2] HP Zhang and HA Makse. Jamming transition in emulsions and granular materials. *Physical Review E*, 72(1):011301, 2005.
- [3] Martin van Hecke. Jamming of soft particles: geometry, mechanics, scaling and isostaticity. *Journal of Physics: Condensed Matter*, 22(3):033101, 2009.
- [4] Corey S O’Hern, Leonardo E Silbert, Andrea J Liu, and Sidney R Nagel. Jamming at zero temperature and zero applied stress: The epitome of disorder. *Physical Review E*, 68(1):011306, 2003.
- [5] Patrick Charbonneau, Eric I Corwin, Giorgio Parisi, and Francesco Zamponi. Jamming criticality revealed by removing localized buckling excitations. *Physical review letters*, 114(12):125504, 2015.
- [6] Matthieu Wyart. Marginal stability constrains force and pair distributions at random close packing. *Physical review letters*, 109(12):125502, 2012.
- [7] Edan Lerner, Gustavo Düring, and Matthieu Wyart. Low-energy non-linear excitations in sphere packings. *Soft Matter*, 9(34):8252–8263, 2013.
- [8] Varghese Babu and Srikanth Sastry. Criticality and marginal stability of the shear jamming transition of frictionless soft spheres. *Physical Review E*, 105(4):L042901, 2022.
- [9] Marco Baity-Jesi, Carl P Goodrich, Andrea J Liu, Sidney R Nagel, and James P Sethna. Emergent SO (3) symmetry of the frictionless shear jamming transition. *Journal of Statistical Physics*, 167(3-4):735–748, 2017.
- [10] Wouter G Ellenbroek, Varda F Hagh, Avishek Kumar, MF Thorpe, and Martin Van Hecke. Rigidity loss in disordered systems: Three scenarios. *Physical review letters*, 114(13):135501, 2015.
- [11] Jose Ortiz, Ethan Stanifer, and Xiaoming Mao. Assur graphs, marginally jammed packings, and reconfigurable metamaterials. *arXiv preprint arXiv:2212.12129*, 2022.
- [12] Dion J. Koeze and Brian P. Tighe. Sticky matters: Jamming and rigid cluster statistics with attractive particle interactions. *Phys. Rev. Lett.*, 121:188002, Nov 2018.
- [13] Dion J. Koeze, Lingtjen Hong, Abhishek Kumar, and Brian P. Tighe. Elasticity of jammed packings of sticky disks. *Phys. Rev. Res.*, 2:032047, Aug 2020.
- [14] DJ Jacobs and MF Thorpe. Generic rigidity percolation in two dimensions. *Physical Review E*, 53(4):3682, 1996.
- [15] MV Chubynsky, M-A Brière, and Normand Mousseau. Self-organization with equilibration: A model for the intermediate phase in rigidity percolation. *Physical Review E*, 74(1):016116, 2006.
- [16] Silke Henkes, David A Quint, Yaouen Fily, and Jennifer M Schwarz. Rigid cluster decomposition reveals criticality in frictional jamming. *Physical review letters*, 116(2):028301, 2016.
- [17] Kuang Liu, Silke Henkes, and JM Schwarz. Frictional rigidity percolation: A new universality class and its superuniversal connections through minimal rigidity proliferation. *Physical Review X*, 9(2):021006, 2019.
- [18] Kuang Liu, Jonathan E Kollmer, Karen E Daniels, JM Schwarz, and Silke Henkes. Spongelike rigid structures in frictional granular packings. *Physical Review Letters*, 126(8):088002, 2021.
- [19] HA Vinutha and Srikanth Sastry. Force networks and jamming in shear-deformed sphere packings. *Physical Review E*, 99(1):012123, 2019.
- [20] HA Vinutha and Srikanth Sastry. Disentangling the role of structure and friction in shear jamming. *Nature Physics*, 12(6):578–583, 2016.
- [21] Varghese Babu, Deng Pan, Yuliang Jin, Bulbul Chakraborty, and Srikanth Sastry. Dilatancy, shear jamming, and a generalized jamming phase diagram of frictionless sphere packings. *Soft Matter*, 17(11):3121–3127, 2021.
- [22] Pallabi Das, HA Vinutha, and Srikanth Sastry. Unified phase diagram of reversible–irreversible, jamming, and yielding transitions in cyclically sheared soft-sphere packings. *Proceedings of the National Academy of Sciences*, 117(19):10203–10209, 2020.
- [23] Nishant Kumar and Stefan Luding. Memory of jamming–multiscale models for soft and granular matter. *Granular Matter*, 18(3):1–21, 2016.
- [24] Peter A Cundall and Otto DL Strack. A discrete numerical model for granular assemblies. *geotechnique*, 29(1):47–65, 1979.

- [25] Steve Plimpton. Fast parallel algorithms for short-range molecular dynamics. *Journal of computational physics*, 117(1):1–19, 1995.
- [26] HA Vinutha, Kabir Ramola, Bulbul Chakraborty, and Srikanth Sastry. Timescale divergence at the shear jamming transition. *Granular matter*, 22(1):1–8, 2020.
- [27] See Supplemental Material at <https://xxx> for the additional information on: I) Details of frictional shear simulation, II) Pebble game algorithm, III) Identifying rattlers, IV) Percolation analysis of the rigid clusters, V) Results with smaller friction coefficient $\mu = 0.1$, VI) Identification of mobilized contacts, VII) Over-constrained networks and floppy modes.
- [28] Kostya Shundyak, Martin van Hecke, and Wim van Saarloos. Force mobilization and generalized isostaticity in jammed packings of frictional grains. *Phys. Rev. E*, 75:010301, Jan 2007.
- [29] Silke Henkes, Martin van Hecke, and Wim van Saarloos. Critical jamming of frictional grains in the generalized isostaticity picture. *EPL (Europhysics Letters)*, 90(1):14003, 2010.
- [30] Jordan L. Shivers, Sadjad Arzash, Abhinav Sharma, and Fred C. MacKintosh. Scaling theory for mechanical critical behavior in fiber networks. *Phys. Rev. Lett.*, 122:188003, May 2019.